A nonlinear terrain-following controller for a VTOL Unmanned Aerial Vehicle using translational optical flow

Bruno Herisse, Tarek Hamel, Robert Mahony, Francois-Xavier Russotto

***Abstract*— This paper presents a nonlinear controller for terrain following of a vertical take-off and landing vehicle (VTOL). The VTOL vehicle is assumed to be a rigid body, equipped with a minimum sensor suite (camera and IMU) along with a measure of the forward speed from another sensor such as global positioning system, maneuvering over a textured terrain made of planar surfaces. Assuming that the forward velocity is separately set to a desired value, the proposed control approach ensures terrain following and guaranties the vehicle does not collide with the ground during the task. The proposed control acquires an optical flow from three spatially separate observation points, typically obtained via three cameras or three non collinear directions in a unique camera. The proposed control algorithm has been tested extensively in simulation and then implemented on a quadrotor UAV to demonstrate the performance of the closed loop system.**

I. INTRODUCTION

The past five years have seen an explosive growth of interest in Unmanned Aerial Vehicles (UAV). Such vehicles have strong commercial potential in automatic or remote surveillance applications such as monitoring traffic congestion, regular inspection of infrastructure such as bridges, dam walls power lines, forest fire or investigation of hazardous environments, to name only a few of the possibilities. There are also many indoors applications such as inspection of infrastructures in mines or large buildings, and search and rescue in dangerous enclosed environments. Historically, payload constraints have severely limited autonomy of a range of micro aerial vehicles. The small size, highly coupled dynamics and 'low cost' implementation of such systems provide an ideal testing ground for sophisticated non-linear control techniques. A key issue arising is the difficulty of navigation through cluttered environments and close to obstructions (obstacle avoidance, take-off and landing). A vision system is a cheap, light, passive and adaptable sensor that can be used along with an Inertial Measurement Unit (IMU) to provide robust relative pose information and more generally allows autonomous navigation. Using a camera as the primary sensor for relative position leads to a visual servo control problem, a field that has been extensively developed over the last few years [1], [2], [3], [4], [5]. An alternate approach for the motion autonomy uses insight from the behavior of flying insects and animals to develop control strategies for aerial robots, in particular, techniques related to visual flow [6]. When a honeybee lands, neither velocity nor distance to the ground are used, the essential information needed is the time-to-contact that can be obtained from the optical flow field divergence [7]. This property has already been used for obstacle avoidance in mobile robotics [8], [9]. Recently control of flying vehicles have been inspired from models of flying insects [8], [9], [10], [11]. Especially, when the optical flow is combined with the forward velocity, several works have been done to provide a measure of the height estimate of the UAV above the terrain followed by altitude control using linear control techniques [12], [13]. The key idea of these works consists in controlling the optical flow so that altitude regulation and terrain following are ensured without guaranteeing obstacle avoidance. It is rare that vehicle dynamics and stability analysis are mentioned in the theoretical developments or even in the experimental discussion of these prior works.

In this paper, we provide a control approach based on the translational optical flow measured by the vehicle for terrain following (or wall following) that ensures obstacle avoidance of an UAV capable of quasi stationary flight. Due to the particular dynamics of the VTOL flight, this task has complexities not present in the analogous task for fixed-wing UAV such as considered by [8]. We consider control of the translational dynamics of the vehicle and in particular focus on regulation of height along with a guarantee that the vehicle will not collide with the ground during transients. A 'high gain' controller is used to stabilise the orientation dynamics; this approach is classically known in aeronautics as guidance and control (or hierarchical control) [14]. The image feature considered is the translational optical flow obtained from the measurement of the optical flow of a textured ground in the inertial frame using additional information provided by an embedded IMU. The ground is reasonably assumed to be made of concatenation of planar surfaces. Lyapunov analysis is used to ensure obstacle avoidance and to prove global asymptotic stability of the closed-loop system for terrain following. The control algorithm has been tested extensively in simulation with success and then implemented on a quadrotor UAV capable of quasi-stationary flight developed by the CEA (French Atomic Energy Commission). Experiments of proposed closed-loop control schemes demonstrate efficiency and performance for terrain following.

The body of the paper consists of seven sections followed by a conclusion. Section II presents the fundamental equations of motion for the quadrotor UAV. In Section III, fundamental equations of optical flow are presented. Sections IV and V present the proposed control strategies for terrain following.

B. Herisse and F.-X. Russotto are with CEA List, Fontenay-Aux-Roses, France firstname.lastname@cea.fr

T. Hamel is with I3S, UNSA - CNRS, Sophia Antipolis, France thamel@i3s.unice.fr

R. Mahony is with Dep. of Eng., Australian Nat. Univ., ACT, 0200 Australia Robert.Mahony@anu.edu.au

Section VI describes simulation results and section VII describes the experimental results obtained on the quadrotor vehicle.

II. UAV DYNAMIC MODEL AND TIME SCALE SEPARATION

The VTOL UAV is represented by a rigid body of mass m and of tensor of inertia $\mathbf{I}$. To describe the motion of the UAV, two reference frames are introduced: an inertial reference frame $\mathcal{I}$ associated with the vector basis $[e_1, e_2, e_3]$ and a body-fixed frame $\mathcal{B}$ attached to the UAV at the center of mass and associated with the vector basis $[e_1^b, e_2^b, e_3^b]$. The position and the linear velocity of the UAV in $\mathcal{I}$ are respectively denoted $\xi = (x, y, z)^T$ and $v = (\dot{x}, \dot{y}, \dot{z})^T$. The orientation of the UAV is given by the orientation matrix $R \in SO(3)$ from $\mathcal{B}$ to $\mathcal{I}$, usually parameterized by Euler's angles ψ, θ, ϕ (yaw, pitch, roll). Finally, let $\Omega = (\Omega_1, \Omega_2, \Omega_3)^T$ be the angular velocity of the UAV defined in $\mathcal{B}$.

A translational force F and a control torque Γ are applied to the UAV. The translational force F combines thrust, lift, drag and gravity components. For a miniature VTOL UAV in quasi-stationary flight one can reasonably assume that the aerodynamic forces are always in direction e_3^b, since the lift force predominates over other components [15]. The gravitational force can be separated from other forces and the dynamics of the VTOL UAV can be written as:

$$\dot{\xi} = v \tag{1}$$

$$m\dot{v} = -TRe_3 + mge_3 \tag{2}$$

$$\epsilon\dot{R} = R\Omega_\times, \tag{3}$$

$$\epsilon\mathbf{I}\dot{\Omega} = -\Omega \times \mathbf{I}\Omega + \Gamma. \tag{4}$$

In the above notation, g is the acceleration due to gravity, and T a scalar input termed the thrust or heave, applied in direction $e_3^b = Re_3$, the third-axis unit vector. The matrix $\Omega_\times$ denotes the skew-symmetric matrix associated to the vector product $\Omega_\times x := \Omega \times x$ for any x.

The positive parameter $\epsilon > 0$ ($\epsilon << 1$) is introduced for timescale separation between the translation and orientation dynamics. It means that the orientation dynamics of the VTOL UAV are compensated with separate high gain control loop. For this hierarchical control, the time-scale separation between the translational dynamics (slow time-scale) and the orientation dynamics (fast-time scale) can be used to design position and orientation controllers under simplifying assumptions. Although reduced-order subsystems can hence be considered for control design, the stability must be analyzed by considering the complete closed-loop system [14]. In this paper, however, we will focus on the control design for the translational dynamics.

III. OPTICAL FLOW EQUATIONS

In this section image plane kinematics and spherical optical flow are derived. The camera is assumed to be attached to the center of mass so that the camera frame coincides with the body-fixed frame.

A. Kinematics of an image point under spherical projection

We compute optical flow in spherical coordinates in order to exploit the passivity-like property discussed in [2]. It is shown in [16] that optical flow equations can be numerically computed from an image plane to a spherical retina. A Jacobian matrix relates temporal derivatives (velocities) in the spherical coordinate system to those in the image frame. Motivated by this discussion, we make the following assumptions.

Assumption 3.1: The image surface of the camera is spherical with unit image radius (f=1).

Assumption 3.2: The target points are stationary in the inertial frame. Thus, motion of target points depends only on motion of the camera.

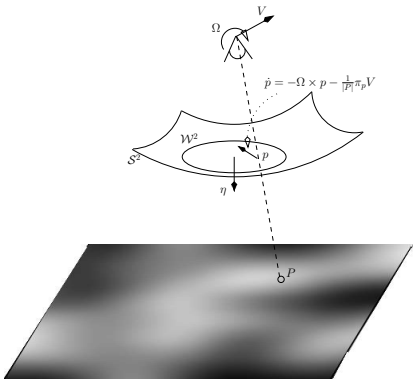

Fig. 1: Image kinematics for spherical camera image geometry

Define $P = (X, Y, Z) \in \Re^3$ as a stationary visible target point expressed in the camera frame. The image point observed by the spherical camera is denoted p and is the projection of P onto the image surface $\mathcal{S}^2$ of the camera. Thus,

$$p = \frac{P}{|P|} \tag{5}$$

The time derivative $\dot{p}$ is the kinematics of the image point, also called optical flow equations, on the spherical surface. The kinematics of an image point for a spherical camera of image surface radius unity are (see [17], [2])

$$\dot{p} = -\Omega \times p - \frac{\pi_p}{|P|}V, \tag{6}$$

Where $\pi_p = (I_3 - pp^T)$ is the projection $\pi_p : \Re^3 \to T_p\mathcal{S}^2$, the tangent space of the sphere $\mathcal{S}^2$ at the point $p \in \mathcal{S}^2$. The vector V represents the translational velocity of the center of mass expressed in the body-fixed frame ($V = R^T v$).

Let $\eta' \in \mathcal{I}$ denote the unit normal taken into a target plane (see [5]) and $\eta = R^T\eta'$ its expression in body-fixed frame $\mathcal{B}$. Define $d := d(t)$, to be the orthogonal distance from the target surface to the origin of frame $\mathcal{B}$, measured as a positive scalar. Thus, for any point P on the target surface

$$d(t) = \langle P, \eta \rangle$$

where both P and η are expressed in the body-fixed frame. One can also write $d(t) = -\langle \eta', \xi \rangle$ where ξ is the position of the camera. For a target point, one has

$$|P| = \frac{d(t)}{\langle p, \eta \rangle} = \frac{d(t)}{\cos(\theta)}$$

where θ is the angle between the inertial direction η and the observed target point p. Substituting this relation into (6) yields

$$\dot{p} = -\Omega_\times p - \frac{\cos(\theta)}{d(t)} \pi_p V \tag{7}$$

B. Translational optical flow computation

Measuring the optical flow is a key aspect of the practical implementation of the control algorithms proposed in the sequel. The optical flow $\dot{p}$ can be computed using a range of algorithms (correlation-based technique, features-based approaches, differential techniques, etc) [18]. Note that due to the rotational ego-motion of the camera, (7) involves the angular velocity as well as the linear velocity [17]. For the control problem we define an inertial translational optical flow from the integral of all observed optical flow corrected for rotational angular velocity. When the observed world is a flat planar surface, inertial translational optical flow will have three components, flow in the two planar directions, analogous to classical optical flow, and flow in the normal direction to the plane, analogous to optical divergence.

Assume that the target plane is textured, the normal direction (η') is known and the available data are $\dot{p}$, η and Ω where η and Ω are estimated from the IMU data (see [19]). The translational optical flow is obtained by integrating the observed optical flow over a section $\mathcal{W}^2$ of the sphere around the pole normal to the target plane (fig. 1). The average of the optical flow along the window $\mathcal{W}^2$ is given by (see appendix for more details):

$$\phi = \iint_{\mathcal{W}^2} \dot{p}\, dp = -\mu \Omega \times \eta - \frac{QV}{d}, \tag{8}$$

where the parameter μ and the matrix Q depend on the size of the window $\mathcal{W}^2$. It can be verified that μ represents the angle of the field of view of the window $\mathcal{W}^2$ and $Q = R^T(R_t \Lambda R_t^T)R$ is a symmetric positive definite matrix. The matrix Λ is a constant diagonal matrix depending on the window $\mathcal{W}^2$ parameters and R_t represents the orientation matrix of the target plane with respect to the inertial frame. For instance, if $\mathcal{W}^2$ is the hemisphere centered at η, corresponding to the visual image of the infinite target plane, it can be shown that ([5])

$$\mu = \pi, \quad \Lambda = \frac{\pi}{4} \begin{pmatrix} 3 & 0 & 0 \\ 0 & 3 & 0 \\ 0 & 0 & 2 \end{pmatrix} \tag{9}$$

From (8) it is straightforward to obtain a measurements of the translational optical flow ($w = \frac{v}{d}$).

$$w = -(R_t \Lambda^{-1} R_t^T) R (\phi + \mu \Omega \times \eta) = \frac{v}{d} \tag{10}$$

IV. A non-linear controller for Terrain Following

In this section a control design ensuring terrain (or wall) following is proposed. The control problem considered is the stabilisation of the distance d about a constant set point d^*. A non-linear controller depending on measurable variables w is developed for the translational dynamics (2). The full vectorial term TRe_3 will be considered as control input for these dynamics. We will assign its desired value $u \equiv (TRe_3)^d = f(w)$. Assuming that actuator dynamics can be neglected before the rigid body dynamics of the UAV, the value T_d is considered to be instantaneously reached by T. Therefore, we have $(TRe_3)^d = TR^d e_3$, where R^d is the desired orientation of the vehicle. This vector can be split into its magnitude, $T = ||f(w)||$, representing the first control input, and its direction $R^d e_3 = \frac{f(w)}{T}$. For the orientation dynamics of (3)-(4), a high gain controller is used to ensure that the orientation R of the UAV converges to the desired orientation R^d. This common approach is used in practice and may be justified theoretically using singular perturbation theory. In the sequel we will focus only on the translational dynamics.

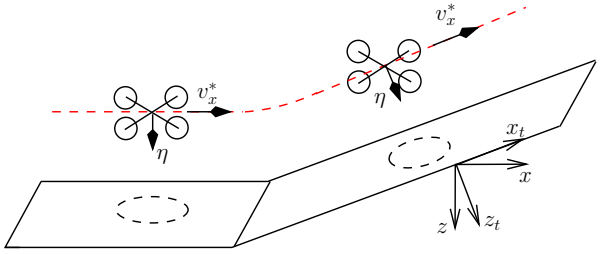

Fig. 2: Terrain following

We will use an existing algorithm, developed within the CEA [20], that uses IMU and vision to estimate the vehicle velocity in 3D. This provides accurate information on the relative motion of the UAV, without providing information on the distance to the ground. We use a linear control to close the loop around velocity regulation perpendicular to the known direction η' and control the dynamics in the direction η' using the optical flow w.

Since the focus of the paper is on the regulation of the vehicle height, we will assume that the error in forward velocity tracking due to the linear controller is negligible. Moreover, without loss of generality, we assume that the motion of the vehicle is in the $x_t - z_t$ plane [1]. That is we assume $\pi_{\eta'} v \equiv (|v_x^*|, 0, 0)$. Note that $\langle v, \eta' \rangle = v_{z_t}$ may be non-zero.

Define

$$w_t^d = R_t^T w^d = (\omega^*, 0, 0)^T, \quad \omega^* > 0,$$

as the desired translational optical flow. Regulation of $w_t \to w_t^d$ certainly ensures that $v_{z_t} = -\dot{d} \to 0$ since $\langle w, \eta' \rangle \to$

[1] the subscript t means that we work on the frame $\mathcal{I}_t$ defined by R_t, that is, $R_t^T \eta' = e_3 \in \mathcal{I}_t$

0 and $d \to |v_x^*|/\omega^* = d^*$. In addition, note that the third component of the translational optical flow w_t acts analogously to optical flow divergence.
Optical flow divergence, depending on $\dot{d}$ can be used as a damping term for the control law. We consider the desired set point ω^* for the flow normal to η' (the flow in direction x_t) and look for a control law that achieves the convergence of d to d^*.

Proposition 4.1: Consider the dynamics of the component of (2) in the direction η' and assume that the component of the thrust vector u_{z_t} ($u_{z_t} \equiv \eta'^T TRe_3$) is the control input. Choose u_{z_t} as follows:

$$u_{z_t} = k_P \left(w_{x_t} - \omega^*\right) + k_D w_{z_t} + \langle mge_z, \eta' \rangle \tag{11}$$

where k_P and k_D are positive parameters. Then for all initial conditions such that $d(0) = d_0 > 0$, the closed-loop trajectory exists for all time and satisfies $d(t) > 0,\ \forall t$. Moreover, $d(t)$ converges asymptotically to d^*.

Proof: Since the dynamics of the considered system are decoupled, recall the dynamics of the component of (2) in the direction η':

$$m\ddot{d} = k_P \left(\frac{|v_x^*|}{d} - \omega^*\right) - k_D \frac{\dot{d}}{d} \tag{12}$$

$$= -k_P |v_x^*| \frac{d - d^*}{d^* d} - k_D \frac{\dot{d}}{d} \tag{13}$$

$$= -k_P \omega^* \frac{\widetilde{d}}{d} - k_D \frac{\dot{d}}{d} \tag{14}$$

Define the Lyapunov function candidate $\mathcal{L}$ by

$$\mathcal{L} = \frac{m}{2}\dot{d}^2 + k_P |v_x^*| \, g\left(\frac{d}{d^*}\right) \geq 0 \tag{15}$$

where,

$$\begin{aligned} g: \quad \Re_+^* &\longrightarrow \Re_+ \\ u &\longmapsto u - \ln u - 1 \end{aligned}$$

It is straightforward to show that for all $u \in \Re_+^*$ and $u \neq 1$, $g(u) > 0$ and $g(1) = 0$. Moreover, g tends to $+\infty$ when u tends to 0 or to $+\infty$.

Differentiating $\mathcal{L}$ and recalling equations (14), it yields

$$\dot{\mathcal{L}} = -k_D \frac{\dot{d}^2}{d} \tag{16}$$

This implies that $\mathcal{L} < \mathcal{L}(0)$ as long as $d(t) > 0$. From the expression of the Lyapunov function, eq. (15), it follows that $\mathcal{L} < \mathcal{L}(0)$ implies there exists $\delta > 0$ such that $d(t) > \delta > 0,\ \forall t$.

Application of LaSalle's principle shows that the invariant set is contained in the set defined by $\dot{\mathcal{L}} = 0$. This implies that $\dot{d} \equiv 0$ in the invariant set. Recalling (14), it is straightforward to show that $\widetilde{d}$ converges asymptotically to 0 and therefore d converges to d^*. ■

Guaranteeing that $d(t)$ remains positive ensures collision free motion along the terrain following. In the above result, it is assumed that the normal direction is known. In the next section, we will show the limits of this result when the normal direction is unknown and how to compute the normal direction using three different measures of the translational optical flow.

Remark 4.2: Note that if the forward velocity is an unknown constant such that $|v_x| > \varepsilon > 0$, obtained for instance by maintaining a constant forward thrust (the drag force opposite to the vehicle's direction of flight ensures that the forward velocity converges to a constant), the altitude controller (11) ensures that d converges to an unknown constant height $d^* > \frac{\varepsilon}{\omega^*}$ while guaranteeing free motion (without collision with the ground). △

V. Case where R_t is unknown a priori

A. Stability of the control law

In this section, we assume that R_t is unknown. Consider the average of the optical flow in a direction $\hat{\eta} \neq \eta$ along a window $\mathcal{W}^2$. Therefore, analogously to equation (10), we compute an optical flow $\hat{w}$:

$$\hat{w} = -(\hat{R}_t \Lambda^{-1} \hat{R}_t{}^T) R(\hat{\phi} + \mu\Omega \times \hat{\eta}) \tag{17}$$

$$= -\hat{R}_t \Lambda^{-1} \hat{\Lambda} \hat{R}_t{}^T \frac{v}{d} \tag{18}$$

In this case, $\hat{\Lambda}$ is not a diagonal matrix (see appendix for more details) and $\Lambda^{-1}\hat{\Lambda}$ can be written as follows:

$$\Lambda^{-1}\hat{\Lambda} = \begin{pmatrix} a & 0 & -\lambda b \\ 0 & a & -\lambda c \\ -\frac{1}{2}b & -\frac{1}{2}c & a \end{pmatrix} \tag{19}$$

where $\lambda = \frac{\mu}{4\pi - \mu}$ and (a, b, c) are defined in the appendix and depend on $\tilde{\alpha} = \alpha - \hat{\alpha}$, $\tilde{\beta} = \beta - \hat{\beta}$. η being unknown, the control law acts in the direction $\hat{\eta}$ and the forward velocity $|v_x^*|$ is regulated on the normal to $\hat{\eta}$. Straightforward but tedious calculations verify that when $\hat{\eta} \neq \eta$, equation (11) can be written as follows ($\pi_{\hat{\eta}'} v = (|v_x^*|, 0, 0)$):

$$m\ddot{d} = -k_P \omega^* \frac{d - Ad^*}{d} a - k_D B \frac{\dot{d}}{d} \tag{20}$$

where A and B are constants depending on $\tilde{\alpha}$, $\tilde{\beta}$, k_P and k_D. Then, it can be shown that, under some conditions on k_P and k_D, d converges to Ad^*. To illustrate this point, simplify the problem and assume that β (the azimuth angle) is known. Then, choose $\hat{\eta}$ such that $\tilde{\beta} = 0$. Therefore, after some calculations,

$$A = \left(\cos(\tilde{\alpha}) + \lambda \sin(\tilde{\alpha}) \tan(\tilde{\alpha}) - \frac{3k_D}{2k_P} \sin(\tilde{\alpha})\right) \tag{21}$$

$$B = \left(\cos(\tilde{\alpha}) - \lambda \frac{k_P}{k_D} \sin(\tilde{\alpha})\right) \tag{22}$$

Using the fact that A and B have to be positive, it is straightforward to verify that the following condition on the gains k_P and k_D

$$\frac{2}{3} \left|\cot(\tilde{\alpha}) + \lambda \tan(\tilde{\alpha})\right| > \frac{k_D}{k_P} > \lambda \left|\tan(\tilde{\alpha})\right| \tag{23}$$

has to be satisfied in order to ensure convergence of d to Ad^*.

B. Estimation of R_t

In this section, we consider extraction of the orientation, R_t, of the target with respect to the inertial frame. We assume that the observed world is made of planar surfaces in order to use results of section III. Straightforward calculations show that we need the computation of $\hat{w}$ in three independent directions $\hat{\eta}_1,\ \hat{\eta}_2,\ \hat{\eta}_3$ to obtain (α, β) and $\frac{v}{d}$. To illustrate this point, simplify the problem and assume that β (the azimuth angle) is known. Then, choose $\hat{\eta}$ such that $\tilde{\beta} = 0$. Thus, only two known directions of calculation will be sufficient. Indeed, compute $\hat{w}$ in two independent directions $\hat{\eta}_1,\ \hat{\eta}_2$ and assume (to simplify) that $\hat{\alpha}_1 - \hat{\alpha}_2 = 90°$. The calculation of $\hat{w}_t = \hat{R}_t^{\ T}\,\hat{w}$ in the two directions gives:

$$\hat{w}_{t1} = \begin{pmatrix} \mathrm{c}\,(\tilde{\alpha}_1) & 0 & -\lambda\,\mathrm{s}\,(\tilde{\alpha}_1) \\ 0 & \mathrm{c}\,(\tilde{\alpha}_1) & 0 \\ -\frac{1}{2}\,\mathrm{s}\,(\tilde{\alpha}_1) & 0 & \mathrm{c}\,(\tilde{\alpha}_1) \end{pmatrix} \frac{\hat{R}_{t1}^{\ T} v}{d} \tag{24}$$

$$\hat{w}_{t2} = \begin{pmatrix} \lambda\,\mathrm{c}\,(\tilde{\alpha}_1) & 0 & -\,\mathrm{s}\,(\tilde{\alpha}_1) \\ 0 & -\,\mathrm{s}\,(\tilde{\alpha}_1) & 0 \\ \mathrm{s}\,(\tilde{\alpha}_1) & 0 & -\frac{1}{2}\,\mathrm{c}\,(\tilde{\alpha}_1) \end{pmatrix} \frac{\hat{R}_{t1}^{\ T} v}{d} \tag{25}$$

Eventually, it is straightforward to obtain α and $\frac{v}{d}$ after some manipulations.

VI. SIMULATIONS

In this section, simulations of the above algorithms designed for the full dynamics of the system are presented. The camera is simulated with a 3D simulator. The UAV is simulated with the model provided by section II. A Pyramidal implementation of the Lucas-Kanade [21] algorithm is used to compute the optical flow. The field of view of the window of computation is $20°$ around the direction of observation $\hat{\eta}$. Optical flow is computed at 384 points on this window. In practice, a least-square estimation of motion parameters is used to obtain robust measurements [22]. However, the following expressions of the matrix Λ and the parameter μ show the sensitivity of the estimation relatively to the field of view:

$$\mu = 0.367 \tag{26}$$

$$\Lambda = \begin{pmatrix} 0.357 & 0 & 0 \\ 0 & 0.357 & 0 \\ 0 & 0 & 0.021 \end{pmatrix} \tag{27}$$

Assuming that $\tilde{\beta} = 0$, two different directions of the translational optical flow are measured and R_t is estimated (V-B). Control Law (11) is used for terrain following. Results present the estimation of α and the trajectory of the UAV. The profile of the terrain is represented in figure 3 by the red dashed line. The slope is set to 25%; it corresponds to $\alpha = 14°$. $|v_x^*|$ is set to $0.5\ m.s^{-1}$ and ω^* is set to $0.1\ s^{-1}$, thus $d^* = 5\ m$. Figures 3 and 4 show results of the simulation. d is the orthogonal distance to the target plane, $\hat{w}_{x_t}$ and $\hat{w}_{z_t}$ (wx and wz in the figure) are respectively measures of the forward and divergent flow. The control law shows good performances and a robust behaviour during transients. Note however that, after several simulations, the estimation of α appears sensitive to noise especially when

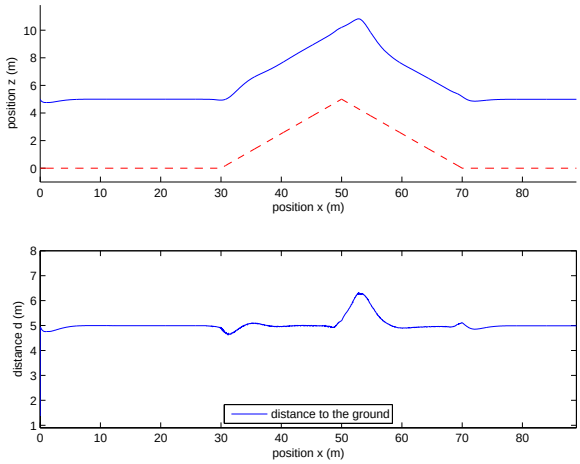

Fig. 3: UAV's trajectory

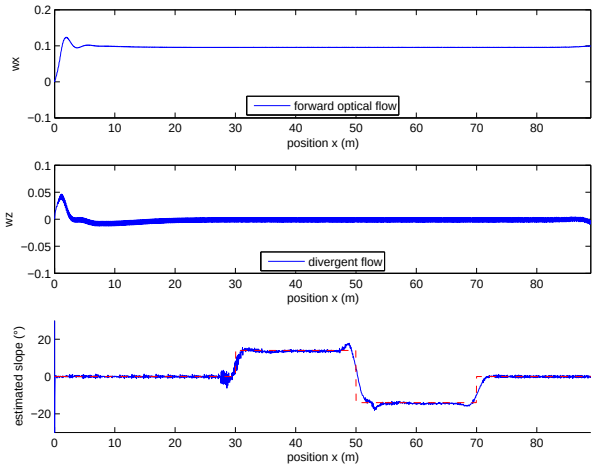

Fig. 4: Estimation of α

the desired optical flow is low but more accurate as long as ω^* is high as shown in figure 4. In order to overcome the problem of the sensitivity to noise, two different solutions may be investigated. The first one consists in increasing the number of measured directions and solving the problem of orientation extraction in an optimisation problem. The second solution, more interesting, consists in providing a dynamic estimator allowing attenuation and filtering of the noise.

VII. EXPERIMENTAL RESULTS

In this section, experimental results of the above algorithm designed for the full height dynamic of the system is presented. The UAV used for the experimentation is the quadrotor, made by the CEA, (Fig. 5) which is a vertical take off and landing vehicle ideally suited for stationary and quasi stationary flight [23].

A. Prototype description

The X4-flyer is equipped with a set of four electronic boards designed by the CEA. Each electronic board includes a micro-controller and has a particular function. The first

board integrates motor controllers which regulate the rotation speed of the four propellers. The second board integrates an Inertial Measurement Unit (IMU) constituted of 3 low cost MEMS accelerometers, which give the gravity components in the body frame, 3 angular rate sensors and 2 magnetometers. On the third board, a Digital Signal Processing (DSP), running at 150 MIPS, is embedded and performs the control algorithm of the orientation dynamics [24] and filtering computations. The final board provides a serial wireless communication between the operator's joystick and the vehicle. An embedded camera with a view angle of 70 degrees pointing directly down, transmits video to a ground station (PC) via a wireless analogical link of 2.4GHz. A Lithium-Polymer battery provides nearly 15 minutes of flight time. The loaded weight of the prototype is about 850g. The images sent by the embedded camera are received by the ground station at a frequency of 25Hz. In parallel, the X4-flyer sends the inertial data to the station on the ground at a frequency of 15Hz. The data is processed by the ground station PC and incorporated into the control algorithm. Desired orientation and desired thrust are generated on the ground station PC and sent to the drone. A key difficulty of the algorithm implementation lies in the relatively large time latency between the inertial data and visual features. For orientation dynamics, an embedded 'high gain' controller in the DSP running at 166Hz, independently ensures the exponential stability of the orientation towards the desired one.

B. Experiments

The considered terrain is made of two parts (it is similar to the representation in figure 2), one part is the ground and the other is a planar surface which make a slope of 25% with the ground. Textures are made of random contrasts (Fig. 5). A Pyramidal implementation of the Lucas-Kanade [21] algorithm is used to compute the optical flow and parameters for the computation are the same as in simulation. The sample time of 15Hz and large time latencies prevent us from experimenting algorithms with high velocities of the quadrotor. Then, to avoid an inaccurate estimation of the slope of the terrain, which could lead to instabilities, we have made the choice to control the UAV without this estimation. Thus, we have to verify the stability of the control law. Recalling results of section V-A along with $\hat{R}_t = I_3$ and $\tilde{\alpha} = 14°$, the parameters k_P and k_D have to be chosen such that the constraint (23) is verified:

$$2.67 > \frac{k_D}{k_P} > 0.0073 \tag{28}$$

$|v_x^*|$ is set to $0.3\ m.s^{-1}$ and ω^* is set to $0.3\ s^{-1}$ and therefore $d^* = 1\ m$. During experiments, the yaw velocity is not controlled. The drone is teleoperated near the target, so that textures are visible. Figure 6 shows the measurement of the forward velocity v_x and the measurement of the forward optical flow w_x. The result shows that $v_x \rightarrow v_x^*$ and $w_x \rightarrow \omega^*$. The distance d cannot be measured (the slope of the target plane is not measured in this experment) but several experiments have been carried out to verify the performance of the approach. One can see that it ensures that the quadrotor follows the terrain without collision. This result can be watched on the video accompanying the paper.

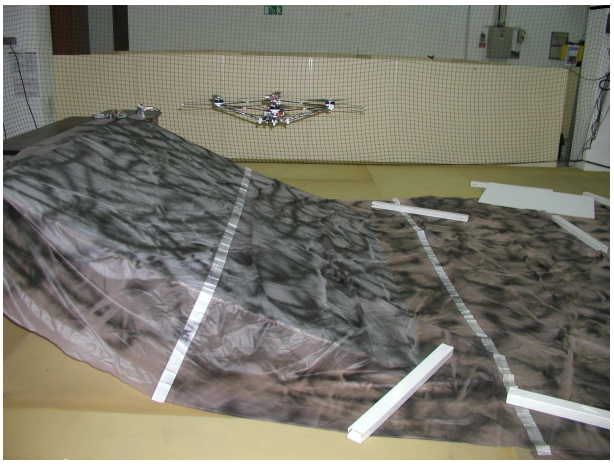

Fig. 5: hovering flight above the textured terrain

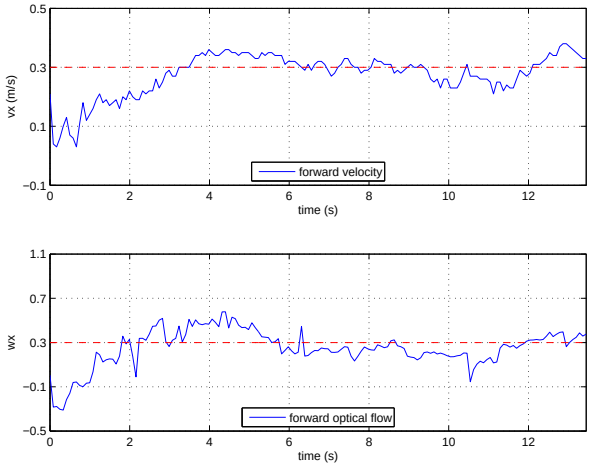

Fig. 6: Forward velocity v_x and forward optical flow w_x

VIII. Concluding remarks

This paper presented a rigorous nonlinear controller for terrain following of a UAV using the measurement of translational optical flow on a spherical camera along with the IMU data. The closed-loop systems and limits of the controller have been theoretically analysed and discussed. The proposed control algorithm has been tested in simulation in different scenarios and then implemented on a quadrotor UAV to demonstrate the performance of the closed loop system.

IX. Acknowledgments

This work was partially funded by Naviflow grant and by ANR project SCUAV (ANR-06-ROBO-0007).

APPENDIX

In this appendix, we provide derivation of optical flow integration. Keep same notations as section III and consider the average of the optical flow in a direction $\hat{\eta} \neq \eta$ along a section $\mathcal{W}^2$ of $\mathcal{S}^2$. Define $(\hat{\alpha}, \hat{\beta})$ the spherical coordinates of $\hat{\eta}$. $\hat{\alpha}$ is the zenith angle and $\hat{\beta}$ is the azimuth angle. Moreover, with this set of parameters, the expression of the orientation matrix, $\hat{R}_t$, of $\hat{\eta}$ with respect to the inertial frame is [2]

$$\hat{R}_t = \begin{pmatrix} \mathrm{c}(\hat{\alpha})\,\mathrm{c}(\hat{\beta}) & -\mathrm{s}(\hat{\beta}) & \mathrm{s}(\hat{\alpha})\,\mathrm{c}(\hat{\beta}) \\ \mathrm{c}(\hat{\alpha})\,\mathrm{s}(\hat{\beta}) & \mathrm{c}(\hat{\beta}) & \mathrm{s}(\hat{\alpha})\,\mathrm{s}(\hat{\beta}) \\ -\mathrm{s}(\hat{\alpha}) & 0 & \mathrm{c}(\hat{\alpha}) \end{pmatrix}$$

Define θ_0 as the half of the field of view of the section $\mathcal{W}^2$. Then:

$$\dot{\hat{\phi}} = \iint_{\mathcal{W}^2} \dot{p} = -\mu\Omega \times \hat{\eta} - \frac{\hat{Q}V}{d},$$

where,

$$\mu = \left| \iint_{\mathcal{W}^2} p\, dp \right| = \pi \sin(\theta_0)^2$$

$Q = R^T(\hat{R}_t \hat{\Lambda} \hat{R}_t^{\,T})R$ is a symmetric positive definite matrix. The matrix $\hat{\Lambda}$ is a symmetric positive definite matrix depending on R_t and $\hat{R}_t$. it can be written as follows:

$$\begin{aligned} \hat{\Lambda} &= \iint_{\mathcal{W}^2} \pi_q \langle p, \eta \rangle\, dq \\ &= \int_{\theta=0}^{\theta_0} \int_{\phi=0}^{2\pi} (I - qq^T) \langle q, \hat{R}_t^{\,T} R\eta \rangle \sin\theta\, d\theta\, d\phi \end{aligned}$$

$q^T = (\mathrm{s}(\theta)\,\mathrm{c}(\phi), \mathrm{s}(\theta)\,\mathrm{s}(\phi), \mathrm{c}(\theta))$. Eventually, straightforward but tedious calculations verify that:

$$\begin{aligned} \hat{\Lambda} &= \frac{\mu^2}{4\pi} \begin{pmatrix} \frac{1}{\lambda}a & 0 & -b \\ 0 & \frac{1}{\lambda}a & -c \\ -b & -c & 2a \end{pmatrix} \\ a &= \mathrm{c}(\alpha)\,\mathrm{c}(\hat{\alpha}) + \mathrm{s}(\alpha)\,\mathrm{s}(\hat{\alpha})\,\mathrm{c}(\tilde{\beta}) \\ b &= \mathrm{s}(\alpha)\,\mathrm{c}(\hat{\alpha})\,\mathrm{c}(\tilde{\beta}) - \mathrm{c}(\alpha)\,\mathrm{s}(\hat{\alpha}) \\ c &= \mathrm{s}(\alpha)\,\mathrm{s}(\tilde{\beta}) \end{aligned}$$

where $\lambda = \frac{\mu}{4\pi - \mu}$ and $\tilde{\alpha} = \alpha - \hat{\alpha}$, $\tilde{\beta} = \beta - \hat{\beta}$. In the particular case where $\hat{\eta} = \eta$, $\tilde{\alpha} = 0$ and $\tilde{\beta} = 0$, the matrix Λ is a diagonal matrix given by

$$\hat{\Lambda} = \Lambda = \frac{\mu^2}{4\pi} \begin{pmatrix} \frac{1}{\lambda} & 0 & 0 \\ 0 & \frac{1}{\lambda} & 0 \\ 0 & 0 & 2 \end{pmatrix}$$

REFERENCES

[1] O. Shakernia, Y. Ma, T. J. Koo, and S. Sastry, "Landing an unmanned air vehicle: vision based motion estimation and nonlinear control," *Asian Journal of Control*, vol. 1, no. 3, pp. 128–146, 1999.

[2] T. Hamel and R. Mahony, "Visual servoing of an under-actuated dynamic rigid-body system: An image based approach," *IEEE Transactions on Robotics*, vol. 18, no. 2, pp. 187–198, 2002.

[3] E. Altug, J. Ostrowski, and R. Mahony, "Control of a quadrotor helicopter using visual feedback," in *Proceedings of the IEEE International Conference on Robotics and Automation*, Washington DC, Virginia, June 2002.

[4] S. Saripalli, J. Montgomery, and G. Sakhatme, "Vision based autonomous landing of an unmanned aerial vehicle," in *Proceedings of the IEEE International Conference on Robotics and Automation*, Washington DC, Virginia, June 2002.

[5] R. Mahony, P. Corke, and T. Hamel, "Dynamic image-based visual servo control using centroid and optic flow features," *Journal of Dynamic Systems Measurement and Control*, vol. 130, no. 1,011005, 2008.

[6] M. Srinivasan, S. Zhang, J. S. Chahl, E. Barth, and S. Venkatesh, "How honeybees make grazing landings on flat surfaces," *Biological Cybernetics*, vol. 83, p. 171183, 2000.

[7] D. N. Lee, "A theory of visual control of braking based on information about time to collision," *Perception*, vol. 5(4), pp. 437–459, 1976.

[8] J.-C. Zufferey and D. Floreano, "Fly-inspired Visual Steering of an Ultralight Indoor Aircraft," *IEEE Transactions on Robotics*, vol. 22, no. 1, pp. 137–146, 2006. [Online]. Available: http://phd.zuff.info

[9] L. Muratet, S. Doncieux, Y. Briere, and J.-A. Meyer, "A contribution to vision-based autonomous helicopter flight in urban environments," *Robotics and Autonomous Systems*, vol. 50, no. 4, pp. 195–209, 2005.

[10] J. S. Chahl, M. V. Srinivasan, and S. W. Zhang, "Landing strategies in honeybees and applications to uninhabited airborne vehicles," *The International Journal of Robotics Research*, vol. 23, no. 2, pp. 101–110, 2004.

[11] F. Ruffier and N. Franceschini, "Visually guided micro-aerial vehicle: automatic take off, terrain following, landing and wind reaction," in *Proceedings of international conference on robotics and automation*, LA, New Orleans, April 2004.

[12] J. S. Humbert, R. M. Murray, and M. H. Dickinson, "Pitch-altitude control and terrain following based on bio-inspired visuomotor convergence," in *AIAA Conference on Guidance, Navigation and Control*, San Francisco, CA, 2005.

[13] F. Ruffier and N. Franceschini, "Optic flow regulation: the key to aircraft automatic guidance," *Robotics and Autonomous Systems*, vol. 50, pp. 177–194, 2005.

[14] S. Bertrand, T. Hamel, and H. Piet-Lahanier, "Stability analysis of an uav controller using singular perturbation theory," in *Proceedings of the 17th IFAC World Congress*, Seoul, Korea, July 2008.

[15] R. Mahony and T. Hamel, "Robust trajectory tracking for a scale model autonomous helicopter," *International Journal of Non-linear and Robust Control*, vol. 14, pp. 1035–1059, 2004.

[16] R. Vassallo, J. Santos-Victor, and H. Schneebeli, "A general approach for egomotion estimation with omnidirectional images," in *OMNIVIS'02*, Copenhagen, Denmark, June 2002.

[17] J. Koenderink and A. van Doorn, "Facts on optic flow," *Biol. Cybern.*, vol. 56, pp. 247–254, 1987.

[18] J. L. Barron, D. J. Fleet, and S. S. Beauchemin, "Performance of optical flow techniques," *International Journal of Computer Vision*, vol. 12, no. 1, pp. 43–77, 1994.

[19] N. Metni, J. Pflimlin, T. Hamel, and P. Souares, "Attitude and gyro bias estimation for a flying uav," in *Proceedings of the IEEE International Conference on Intelligent Robots and Systems*, Edmonton, Canada, 2005.

[20] N. Guenard, "Optimisation et implémentation de lois de commande embarquées pour la téléopration intuitive de micro drones aériens "x4-flyer"," Ph.D. dissertation, université Nice Sophia Antipolis, 2007.

[21] B. Lucas and T. Kanade, "An iterative image registration technique with an application to stereo vision," in *Proceedings of the Seventh International Joint Conference on Artificial Intelligence*, Vancouver, 1981, pp. 674–679.

[22] S. Umeyama, "Least-squares estimation of transformation parameters between two point patterns," *IEEE Trans. PAMI*, vol. 13, no. 4, pp. 376–380, 1991.

[23] N. Guenard, T. Hamel, and R. Mahony, "A practical visual servo control for an unmanned aerial vehicle," *IEEE Transactions on Robotics*, vol. 24, pp. 331–340, 2008.

[24] N. Guenard, T. Hamel, V. Moreau, and R. Mahony, "Design of a controller allowed the intuitive control of an x4-flyer," in *SYROCO'06*, University of Bologna, Italy, 2006.

[2] for all $x \in \Re, \mathrm{s}(x) = \sin(x),\ \mathrm{c}(x) = \cos(x),\ \mathrm{t}(x) = \tan(x)$